Faraday Discussions

Accepted Manuscript

This manuscript will be presented and discussed at a forthcoming Faraday Discussion meeting. All delegates can contribute to the discussion which will be included in the final volume.

Register now to attend! Full details of all upcoming meetings: http://rsc.li/fd-upcoming-meetings

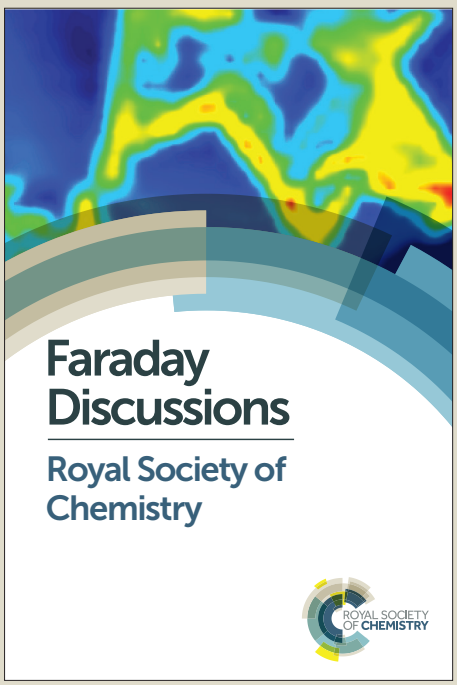

This is an *Accepted Manuscript*, which has been through the Royal Society of Chemistry peer review process and has been accepted for publication.

Accepted Manuscripts are published online shortly after acceptance, before technical editing, formatting and proof reading. Using this free service, authors can make their results available to the community, in citable form, before we publish the edited article. We will replace this *Accepted Manuscript* with the edited and formatted *Advance Article* as soon as it is available.

You can find more information about *Accepted Manuscripts* in the Information for Authors.

Please note that technical editing may introduce minor changes to the text and/or graphics, which may alter content. The journal's standard Terms & Conditions and the Ethical guidelines still apply. In no event shall the Royal Society of Chemistry be held responsible for any errors or omissions in this *Accepted Manuscript* or any consequences arising from the use of any information it contains.

ROYAL SOCIETY OF CHEMISTRY

www.rsc.org/faraday_d

A Mechanistic Model for Oxide Growth and Dissolution during Corrosion of Cr-Containing Alloys

M. Momeni, J.C. Wren
Department of Chemistry, the University of Western Ontario
London, Ontario, Canada N6A 5B7
jcwren@uwo.ca

Abstract

We have developed a corrosion model that can predict metal oxide growth and dissolution rates as a function time for a range of solution conditions. Our model considers electrochemical reactions at the metal/oxide and oxide/solution interfaces, and the metal cation flux from the metal to the solution phase through a growing oxide layer, and formulates the key processes using classical chemical reaction rate or flux equations. The model imposes mass and charge balance and hence, is labeled as the Mass Charge Balance (MCB) model. Mass and charge balance dictate that at any given time the oxidation (or metal cation) flux must be equal to the sum of the oxide growth flux and the dissolution flux. For each redox reaction leading to the formation of a specific oxide, the metal oxidation flux is formulated using a modified Butler-Volmer equation with an oxide-thickness-dependent effective overpotential. The oxide growth and dissolution fluxes have a first-order dependence on the metal cation flux. The rate constant for oxide formation also follows an Arrhenius dependence on the potential drop across the oxide layer and hence decreases exponentially with oxide thickness. This model is able to predict the time-dependent potentiostatic corrosion behaviour of both pure iron, and Co-Cr and Fe-Ni-Cr alloys.

Keywords: Model; Oxide Growth; Dissolution; Corrosion; Cr-containing alloys;

List of Acronyms and Symbols

V	Driving force for corrosion (V)
$E_{rdx\#}^{eq}$	Equilibrium potential of a redox pair # involved in corrosion (V)
E_{corr}	Corrosion potential (V)
E_{app}	Applied potential during polarization (V)
$E_{rdx\#}(t)$	Electrochemical potential of the reacting system at time *t* (V)
$E_{ox\#}^{eq}$	Equilibrium potential for oxidation half-reaction (V)
$E_{red\#}^{eq}$	Equilibrium reduction half reaction potential (V)
$E_{elec}(t)$	Electrode potential at time *t*. It is E_{corr} in an open circuit and E_{app} in potentiostatic polarization (V)
$\eta_{rdx\#}(t)$	Overpotential at the reaction interface (V)
$\eta_{ox\#}(t)$	Anodic overpotential (V)
$\eta_{red\#}(t)$	Cathodic overpotential (V)
$i_{rdx\#}^{eq}$	Exchange current density ($A{\cdot}cm^{-2}$)
$i_{rdx\#}(t)$	Current density at time *t* ($A{\cdot}cm^{-2}$)
n	Number of electrons involving in the reaction.
$\alpha_{rdx\#}$	Transfer coefficient or symmetry factor, normally equal to 0.5
F	Faraday's constant (96485 $C{\cdot}mol^{-1}$)
R	Universal gas constant (8.314 $J{\cdot}mol^{-1}{\cdot}K^{-1}$)
T	Absolute temperature (K)
$m\|ox$	Metal/oxide interface
$ox\|sol$	Oxide/solution interface
$\varphi_{m\|ox}$	Fermi level at the metal oxide interface (V)
$\varphi_{ox\|sol}$	Fermi level at the oxide solution interface (V)
$\Delta\varphi_{oxide}(\mathrm{t})$	Potential drop across the oxide layer at time t (V)
$J_{M\#^{n+}}(t)\|_{m\|ox}$	Metal oxidation flux at the metal/oxide interface ($mol{\cdot}s^{-1}{\cdot}cm^{-2}$)
$J_{red\#}(t)\|_{ox\|sol}$	Solution reduction flux ($mol{\cdot}s^{-1}{\cdot}cm^{-2}$)
$\langle J_{M^{n+}}(z,t)\rangle_{oxide}$	Average flux of metal cations across the oxide layer ($mol{\cdot}s^{-1}{\cdot}cm^{-2}$)
$J_{M\#^{n+}}(t)\|_{ox\|sol}$	Total flux of metal cations arriving at the ox|sol interface ($mol{\cdot}s^{-1}{\cdot}cm^{-2}$)
$J_{MO\#}(t)\|_{oxide}$	Oxide growth flux ($mol{\cdot}s^{-1}{\cdot}cm^{-2}$)
$J_{diss\#}(t)\|_{sol}$	Dissolution flux ($mol{\cdot}s^{-1}{\cdot}cm^{-2}$)
$L_{MO\#}(t)$	Thickness of the MO# oxide layer (cm)
$-\Delta_r G(t)$	Free energy of reaction ($J{\cdot}mol^{-1}$)
φ_m^{eq}	Fermi level of metal at equilibrium
φ_{sol}^{eq}	Fermi level of solution at equilibrium
$\varphi_{E(Ox)}$	Density of unoccupied electron energy states of oxidants
$\varphi_{E(red)}$	Density of occupied electron energy states of reduction reaction products
$\varphi_{E(M^{n+})}$	Density of unoccupied electron energy states of metal cation
$\varphi_{E(M)}$	Density of occupied electron energy states of metal atom
φ_{CB}	Lowest energy of conduction band
φ_{VB}	Highest energy of valance band

$\varepsilon_{MO\#}$	Specific potential gradient of oxide ($V \cdot cm^{-1}$)
$\Delta Ea_{MO\#}(t)$	Activation energy barrier for oxide growth at time t ($J \cdot mol^{-1}$)
$\Delta Ea_{MO\#}(0)$	Activation energy barrier for oxide growth at time t = 0 (no oxide on the surface) ($J \cdot mol^{-1}$)
$\Delta Ea_{oxide}(t)$	Activation energy barrier for oxide growth across the oxide present on the surface at time t ($J \cdot mol^{-1}$)
$c_{MO\#}$	Specific activation energy gradient of oxide ($J \cdot mol^{-1} \cdot cm^{-1}$)
A_{sol}	Surface area exposed to solution (cm^2)
$m_{diss\#}$	Dissolved amount of metal cations (mol)
$\Delta V_{oxide}(t)$	Potential drop across an oxide layer at time t (V)
$\Delta V_{oxide}(0)$	Potential drop across an oxide layer at time zero (V)
$\Delta V_{MO\#}(t)$	Potential drop across the layer of MO# at time t (V)
$\upsilon_{MO\#}$	Molar volume of oxide ($cm^3 \cdot mol^{-1}$)
L_{Cr2O3}	Thickness of air-formed chromium oxide (cm)
L_{MCr2O4}	Thickness of growing chromite (cm)
f_l	Relative monolayer length of Cr_2O_3 to chromite
$f_{k\text{-}MO\#}$	Relative ratio of the oxide formation and dissolution constants
$\lambda_{MO\#}$	Constant related to the potential drop in the oxide (cm^{-1})
J_{MO}"	Constant component of metal cation flux

1. INTRODUCTION

Several corrosion models have been developed for predicting the rate of metal dissolution in the presence of an oxide film[1-13]. To obtain the rate of corrosion under a given driving force (V), many of these models focus on solving the transport rate equations for individual charge carriers (interstitial cations and anions, cation and anion vacancies, and electrons and holes) across the oxide film, in addition to the rates of their creation at respective interfaces (i.e. electrochemical redox reaction rates). Since the rate of charge transport (charge flux) depends on the electric field gradient (electric potential), the electrochemical potentials of the metal, the oxide and the solution phases are important parameters in determining the corrosion rate. These potentials may change with time as corrosion progresses. However, these models do not specifically define the driving force for corrosion as a function of quantifiable potentials such as the equilibrium potential of a redox pair involved in corrosion (E_{rdx}^{eq}), or the electrode potential (corrosion potential (E_{corr}) on open circuit, or the applied potential (E_{app}) during polarization).

In these models, the distribution of the driving force for corrosion on a corroding surface is often presented schematically as shown in Figure 1. The implicit assumptions in this schematic are that the driving force for corrosion (V) is the potential difference between the Fermi levels in the metal and the solution phases, that the driving force is distributed between the metal/oxide (m|ox) and oxide/solution (ox|sol) interfaces and the oxide film present, and that the potential may not be constant across the oxide film. The models differ in their assumptions on how the driving force is distributed and on how the potential distribution changes as the oxide film grows. For example, the potential drop across an oxide film is assumed to be independent of oxide thickness in the Cabrera-Mott model[4], while it increases with oxide thickness in other models[9-13]. Alternatively the potential difference at the ox|sol interface may be assumed to be constant as the

oxide grows (the Point Defect Model (PDM))[9] while the potential difference at the m|ox interface is assumed to be constant in the Generalized Model for Oxide Film Growth[12, 13].

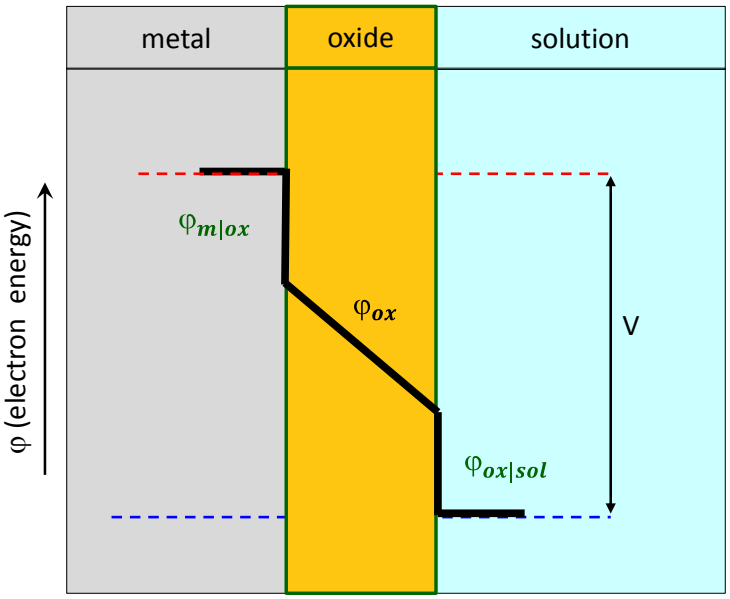

Figure 1: Commonly accepted scheme for the distribution of the potential difference between the metal and solution phases, V, in a metal/oxide/solution system.

In addition, these models do not explicitly express the potentials that control the charge transport rates as a function of quantifiable potentials such as E_{corr} or E_{rdx}^{eq}. The models assign different rates for the transport of different charge carriers across the solid oxide phase (ions, ion vacancies, electrons and holes). The individual transport rate parameters are difficult to verify, and this limits the predictive capabilities and the application ranges of these models. Oddly, mass and charge balance for the overall corrosion process, clear physical requirements, are not generally invoked in these models.

We have developed a corrosion kinetic model that can simulate both oxide film growth and metal dissolution as a function of time for a range of potentials, pHs and temperatures. Our model considers many of the elementary processes that are included in other models:

electrochemical redox reactions at the m|ox and ox|sol interfaces, the transport of charged species across the oxide film, metal oxide formation and growth, and metal ion dissolution. The rates of the individual elementary reactions/processes are formulated using classical chemical reaction rate, and mass and charge flux equations. However, our model imposes mass and charge balance requirements on these rates, and reaction thermodynamic and kinetic constraints on electrochemical redox reactions. Hence we have labeled our model the Mass Charge Balance (MCB) model.

In this paper, we describe the fundamental physical and chemical processes that underlie the MCB model and show how it can predict both oxide growth and dissolution during corrosion of an alloy. The rationales for the MCB model assumptions and the rate or charge flux equations used in the model are presented. In particular, we establish the driving force for corrosion as a function of equilibrium potential and how the driving force is distributed among the m|ox and ox|sol interfaces and across the oxide layer. The model includes relationships between the potential drop across the oxide film and the film thickness, and between the potential drop and the activation energy for oxide formation, and the rate of oxide growth as a function of the oxide thickness. We present a few comparisons of model simulations of the time-dependent corrosion current and oxide growth during potentiostatic polarization with data obtained for pure iron (using data from Sato et al.[14]) and for Cr-containing alloys: a Co-Cr alloy, Stellite 6[15], and an Fe-Ni-Cr alloy, Alloy 800.

2 The MCB Model

2.1 Overview of the MCB Model

The MCB model considers corrosion to consist of four elements: electrochemical redox reactions at the m|ox and ox|sol interfaces, the transport of charged species across the oxide film,

metal oxide formation and growth, and metal ion dissolution. The rates of the individual elementary reactions/processes in the model are formulated using classical chemical reaction rate, and mass and charge flux equations. The MCB model imposes mass and charge balance requirements on these rates, and reaction thermodynamic and kinetic constraints on electrochemical redox reactions. The mass and charge balance requirements invoked in the MCB model dictate that the rate of metal oxidation must equal the rate of its coupled solution species reduction, and the rate of metal oxidation must equal the sum of the rates of oxide formation and metal dissolution. This allows us to avoid the need for detailed modeling of charge transport across the oxide film. Instead, the MCB model takes into account the dependence of the potential drop across the oxide film on the type and thickness of the oxide(s) that grow with time.

Metal alloys may contain more than one active element that may form an oxide or hydroxide. This oxide can contain only a single metal element, or it can be a mixed oxide/ hydroxide with more than one metal element. In addition, transition metals have many stable oxidation states and this, combined with the possibility of forming several different stable oxides and hydroxides, leads to the possible formation of many different layers of oxides/hydroxides on a metal surface. The MCB model recognizes that different metal oxides can form and that the oxide composition and structure may change as corrosion progresses[15, 16]. The result can be a complex and shifting set of oxides that form and grow as a function of time, even at a fixed potential[15]. The different types of metal oxides can have different oxide layer resistances and this will affect the potential drop across the oxide, and evolution in the nature of the oxide layer with time will change the potential drop as a function of time.

Irrespective of the type of oxide that forms and the rate of its formation, oxide formation is an electrochemical reaction and constrained by reaction thermodynamics. The thermodynamic

constraints invoked in the MCB model dictate that metal oxidation (coupled with solution reduction) leads to formation of a certain type of oxide with a driving force given by the difference in the equilibrium potentials of the two coupled redox half-reactions for that process. Energy pathway minimization prevents an oxide that requires a higher free energy of reaction from forming in competition. The MCB model assumes that the thermodynamic driving force is distributed between the m|ox and ox|sol interfaces and the oxide layer, in a manner somewhat similar to that shown in Figure 1. Due to the potential distribution, the effective driving force for metal oxidation decreases as the oxide grows. In the MCB model the distribution of the driving force at the m|ox and ox|sol interfaces and across the oxide layer is dictated by the mass and charge balance requirements. That is, the potential is distributed such that the rate of metal oxidation that produces metal cations must be the same as the rate of the metal cations moving across the oxide film, and these rates must be the same as the sum of the rates of metal oxide formation and metal ion dissolution.

The MCB model assumes that for a given type of oxide there is a charge distribution across the oxide layer (there is a higher metal cation concentration near the m|ox interface and a higher oxygen anion concentration near the ox|sol interface). In this case the oxide film on a corroding surface resembles a p-n junction in a solid-state diode device and is not a uniform semiconductor. Consequently, the potential drop across an oxide layer ($\Delta V_{oxide} = -\Delta\varphi_{oxide}$) increases linearly with oxide thickness. An increase in ΔV_{oxide} decreases the effective overpotentials for the redox half-reactions at the two interfaces. The result is that the metal oxidation rate can be formulated using a modified Butler-Volmer equation with an effective overpotential, provided that one can define the linear rate of oxide growth with time.

The MCB model assumes that the rate of oxide growth has a first order dependence on the flux of metal cations and that the oxide growth rate constant has an Arrhenius dependence on the activation energy for the metal oxide formation. The activation energy increases with an increase in ΔV_{oxide}, and hence, the rate constant for metal oxide formation decreases exponentially with an increase in oxide thickness.

The last key component of the MCB model takes into account the competition between oxide formation and dissolution for the metal cations produced by metal oxidation. Due to the mass and charge balance requirements the rate of metal oxidation must be the same as the sum of the rates of metal oxide formation and dissolution. In contrast to the changing oxide growth rate with oxide thickness, the rate constant for metal dissolution at the ox|sol interface is generally assumed to be independent of oxide thickness, but dependent on the type of dissolving oxide and the metal cation dissolution properties of the contacting solution (pH, temperature, etc.).

The principles behind the MCB model assumptions and the formulation of the rate equations are described next.

2.2 Elementary Electrochemical and Transport Processes

The elementary physical processes considered in the MCB model are schematically presented in Figure 2[15]. Metal oxidation occurs at the m|ox interface (Process 1a) and the reduction of aqueous species occurs on a counter electrode (Process 1b). On a naturally corroding surface (an open circuit) both the metal oxidation and the aqueous species reduction occur on the same (on a macroscopic scale) surface. When an alloy electrode is polarized in an electrochemical cell the two redox reactions occur on separated surfaces. The redox half-reactions are coupled via a flux of metal cations from the m|ox interface to the ox|sol interface (Process 2). The metal cations at the ox|sol interface can be hydrated and dissolve into the

solution (Process 3), or combine with oxygen anions in the solution (O^{2-} or OH^-) to form a solid metal oxide that attaches to the ox|sol interface (Process 4). In this schematic, the metal cations are depicted as moving from the m|ox interface to the ox|sol interface. This does not mean that the individual metal cations physically move through the oxide layer, but rather that there is relative movement of the interfaces with respect to each other. Oxygen anions moving from the ox|sol to the m|ox interface results in the same transport rate equation. The net result is the transfer of metal species from the metal phase to the solution phase.

The oxyhydroxides of transition metals typically exhibit semiconducting properties[17]. For a chemically inert semiconductor, charge transport through the semiconductor is normally accomplished by movement of electrons (for an n-type) and holes (for a p-type). On a corroding metal surface, transfer of more massive charged species (metal cations and/or oxygen anions) also occurs. Movement of relatively massive ions through a solid oxide phase is not easy. To account for the charge flux through a solid oxide lattice, many mechanisms, such as transport of metal cations (or oxygen anions) via interstitials, or cation and anion vacancies, and electron hopping (or ion exchanges), have been proposed[4, 5, 9, 11-13]. Irrespective of the ion transport mechanism, the charge flux through a corroding surface can be modeled as the net flux of metal cations from the m|ox interface to the ox|sol interface.

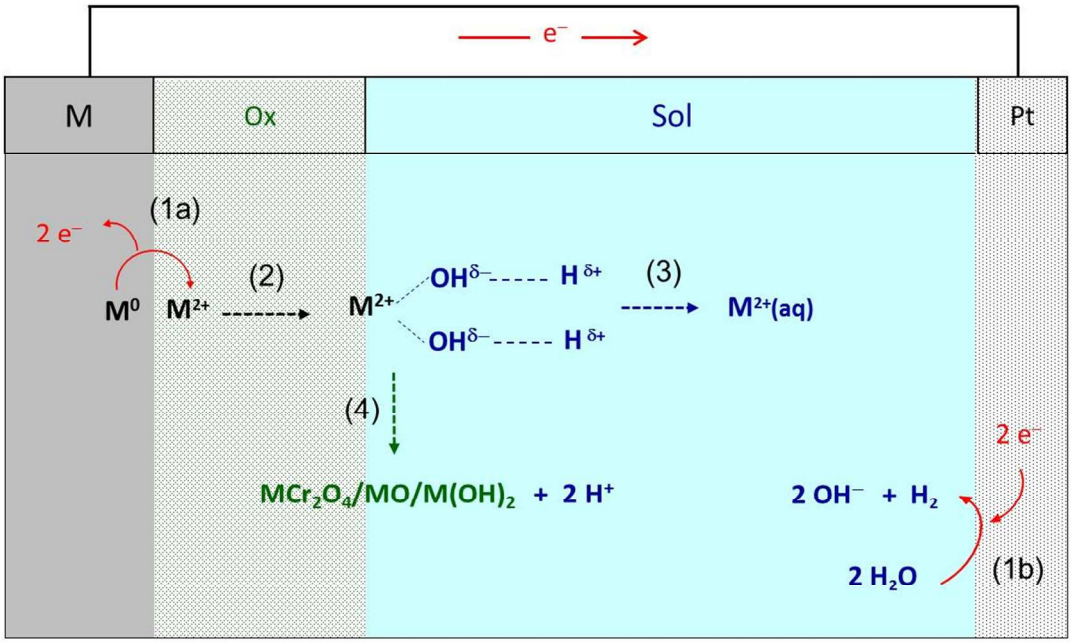

Figure 2: Schematic of the elementary processes considered in the MCB model.

For simplicity, only one active metal element, M, and its oxidation to one oxidation state M^{2+} are shown in Figure 2. Similarly, only water is reduced. However, for an alloy the set of elementary reactions will be much larger, taking into account all of the metal components of the alloy and their possible stable oxidation states, and the solution redox conditions. For example, in a highly oxidizing solution (e.g., containing H_2O_2) the oxide growth process (Process 4) on a Ni-Fe-Cr alloy may consist of (1) oxidative conversion of an pre-existing layer of defective Cr_2O_3 to $FeCr_2O_4$, followed by (2) formation and growth of Fe_3O_4 and $NiFe_2O_4$ and then (3) formation and growth of $NiO/Ni(OH)_2$[16]. On a Co-Cr alloy Process 4 may consist of (1) conversion of pre-existing Cr_2O_3 to $CoCr_2O_4$, followed by (2) formation and growth of $CoO/Co(OH)_2$ and then (3) formation and growth of CoOOH and Co_3O_4[15].

2.3 Mass and Charge Balance

In the MCB model, the rates of individual reactions/processes are formulated using classical chemical reaction rate and mass and charge flux equations. The rates of the individual processes shown in Figure 2 cannot vary independently. The mass and charge balance requirements dictate that at any given time, the rate of metal oxidation must satisfy

Oxidation rate = rate (1a) = rate (1b) = rate (2) = rate (3) + rate (4) (1)

The mass balance dictates that the rates of the reactions that occur in series must be the same. Also the total rate of reactions in parallel is the sum of the individual reaction rates. Hence, the slowest in a series of reactions dictates the oxidation rate while dissolution (3) and oxide formation (4) in parallel compete for the metal cations.

For processes occurring at an interface the rates are better expressed in terms of fluxes than in term of the change in concentration of a species (although the flux may depend on concentration gradient of a species at the interface). Furthermore, in electrochemical studies of corrosion, the current (charge flux) is the measured quantity. The mass and charge balance requirements in terms of charge flux are:

(a) The flux of positive charges from the metal to the oxide phase at the m|ox interface (Process 1a) must be equal to the flux of negative charges from the solution to oxide phase at the ox|sol interface (Process 1b). Hereafter, these fluxes are referred to as the metal oxidation flux, $J_{M\#^{n+}}(t)|_{m|ox}$ and the solution reduction flux, $-J_{red\#}(t)|_{ox|sol}$, respectively.

$$J_{M\#^{n+}}(t)|_{m|ox} = -J_{red\#}(t)|_{ox|sol} \quad (2)$$

where the fluxes are in units of mol·s^{-1}·cm^{-2}.

(b) The metal oxidation flux at the m|ox interface must be equal to the average flux of the metal cations across the oxide phase, $\langle J_{M^{n+}}(z,t)\rangle_{oxide}$, (Process 2) and hence the total flux of metal cations arriving at the ox|sol interface:

$$J_{M\#^{n+}}(t)|_{m|ox} = \langle J_{M\#^{n+}}(z,t)\rangle_{oxide} = J_{M\#^{n+}}(t)|_{ox|sol} \quad (3)$$

The flux of the metal cations may vary along the oxide layer but the MCB model does not formulate this in detail. The average flux is assumed to be inversely proportional to the thickness of the oxide layer, $L_{oxide}(t)$, that may be initially present or growing

$$\langle J_{M\#^{n+}}(z,t)\rangle_{oxide} = \frac{1}{L_{MO}(t)} \cdot \left(\int_0^{L_{MO}(t)} J_{M\#^{n+}}(z,t) \cdot dz\right) \quad (4)$$

Again it should be emphasized that a flux of the metal cations from the m|ox to ox|sol interface does not mean the physical movement of individual cations through the solid oxide phase but rather the relative movement of the interfaces with respect to each other. The flux of the oxygen anions from the ox|sol to m|ox interface in the opposite direction yields the same flux equation for positive charges.

(c) The charge flux must be equal to the sum of the fluxes of metal cations that dissolve into the solution phase (Process 3) and those that are used for growing an oxide film (Process 4)

$$J_{M\#^{n+}}(t)|_{ox|sol} = J_{diss\#}(t)|_{sol} + J_{MO\#}(t)|_{oxide} \quad (5)$$

and these are referred to as the dissolution flux, $J_{diss\#}(t)|_{sol}$, and the oxide growth flux, $J_{MO\#}(t)|_{oxide}$, respectively.

The condition of equal fluxes for metal oxidation and solution reduction dictates the potential on a naturally corroding surface (E_{corr}) with the net current at E_{corr} being zero. Under polarization, the rate of oxidation (or reduction) occurring on the working electrode must equal the rate of reduction (or oxidation) occurring on the counter electrode, and this rate depends on the polarization potential (E_{app}).

In the MCB model we formulate the metal oxidation flux, $J_{M\#^{n+}}(t)|_{m|ox}$, and the oxide growth flux, $J_{MO\#}(t)|_{oxide}$, as functions of corrosion parameters (potentials, pH, T, etc.) and the other fluxes are determined using the mass and charge balance equations (equations 1 to 5).

In formulating $J_{M\#^{n+}}(t)|_{m|ox}$ and $J_{MO\#}(t)|_{oxide}$, the MCB model takes the free energy of reaction for the redox reaction forming a specific oxide MO as the driving force (or reaction potential) for the reaction. The driving force is then distributed between the m|ox and ox|sol interfaces and the oxide film present on the surface. How the potential is distributed between the three components is discussed in Section 2.5.

Equal rates for metal oxidation and the sum of the metal oxide formation and metal ion dissolution rates then dictates the rate of oxide growth and its dependence on pH and temperature. Since metal oxidation results in both metal cation dissolution and oxide formation, the competing kinetics of these two pathways affects the rate of oxide growth[15, 16]. These fluxes are discussed in Section 2.6.

2.4 Formulation of the Metal Oxidation Flux, $J_{M\#^{n+}}(t)|_{m|ox}$

The overall redox reaction of M during corrosion can be expressed as,

$$M + Ox \leftrightarrows M^{n+} + Red \quad (6)$$

where Ox represents the solution oxidant and Red represents its reduced species. Knowing the nature of the metal and the solution redox species we can calculate the Gibbs free energy of this reaction. The driving force for the overall reaction (the free energy of reaction, $-\Delta_r G(t)$) is the difference in electrochemical potential of the reacting system at time t ($E_{rdx}(t)$) and at equilibrium (E_{rdx}^{eq}):

$$-\Delta_r G(t) = -n \cdot F \cdot \Delta_r E(t) \quad (7a)$$

$$-\Delta_r G(t) = n \cdot F \cdot \left(E_{rdx}(t) - E_{rdx}^{eq}\right) \quad (7b)$$

By convention the electrochemical potential scale uses the reduction potential with respect to the standard hydrogen electrode potential (SHE), but the scale zero point is not important. A chemical reaction depends on the difference in potential and not the absolute values of the potentials.

The overall redox reaction is often expressed using two half-reactions:

Ox: $M \leftrightarrows M^{n+} + n\, e^-$ (8a)

Red: $Ox + n\, e^- \leftrightarrows Red$ (8b)

This division is used for convenience in evaluating reaction thermodynamics. The electrochemical equilibrium potential for the overall redox reaction (6) can then be expressed using the equilibrium potentials of the two half-reactions,

$$\Delta E_{rdx}^{eq} = E_{red}^{eq} - E_{ox}^{eq} \quad (9a)$$

On the potential scale with respect to V_{SHE} this becomes

$$\Delta E_{rdx}^{eq} = E_{rdx}^{eq}(V_{SHE}) \quad (9b)$$

For an electrochemical reaction of a specific redox pair, *rdx#*, the net rate of the reaction (or the net flux of charges) can be defined by the Butler-Volmer equation. In terms of current:

$$i_{rdx\#}(t) = i_{rdx\#}^{eq} \cdot \left(exp\left(\frac{n \cdot F}{RT} \cdot \alpha_{rdx\#} \cdot \eta_{rdx\#}(t)\right) - exp\left(-\frac{n \cdot F}{RT} \cdot (1 - \alpha_{rdx\#}) \cdot \eta_{rdx\#}(t)\right)\right) \quad (10a)$$

$$\eta_{rdx\#}(t) = E_{elec}(t) - E_{rdx\#}^{eq} \quad (10b)$$

where $i_{rdx\#}^{eq}$ is the exchange current, or the anodic or cathodic current at equilibrium, n is the number of electrons involved in the reaction, $\alpha_{rdx\#}$ is the transfer coefficient (typically with a value of 0.5), F is Faraday's constant, R is universal gas constant (8.314 $J \cdot mol^{-1} \cdot K^{-1}$), T is absolute temperature (K), $\eta_{rdx\#}(t)$ is the overpotential at the reaction interface, and $E_{elec}(t)$ is

the electrode potential or the potential at the reaction interface at time t. The electrode potential is the potential that we measure as the corrosion potential, E_{corr}, on an open circuit or the applied potential, E_{app}, on polarization. When $E_{elec}(t)$ is sufficiently more positive or more negative than the equilibrium potential $E_{rdx\#}^{eq}$, the Butler-Volmer equation can be approximated to:

$$i_{rdx\#}(t) \approx i_{ox\#}(t) = i_{ox\#}^{eq} \cdot \left(exp\left(\frac{0.5 \cdot n \cdot F}{RT} \cdot \eta_{ox\#}(t) \right) \right) \quad \text{for } \eta_{rdx\#}(t) > 0 \qquad (11a)$$

$$i_{rdx\#}(t) \approx i_{red\#}(t) = i_{red\#}^{eq} \cdot \left(-exp\left(-\frac{0.5 \cdot n \cdot F}{RT} \cdot \eta_{red\#}(t) \right) \right) \quad \text{for } \eta_{rdx\#}(t) < 0 \qquad (11b)$$

where $i_{rdx\#}^{eq} = i_{ox\#}^{eq} = -i_{red\#}^{eq}$ (11c)

$$\eta_{rdx\#}(t) = \eta_{ox\#}(t) = -\eta_{red\#}(t) \qquad (11d)$$

The transfer coefficient is often empirically determined for a particular corrosion process[18]. In the MCB model the transfer coefficient for each elementary redox reaction, *rdx#*, is fixed at 0.5 and is not an adjustable parameter.

On a bare metal surface, there is only one reaction interface, the metal/solution interface, and the overpotential at the interface is defined as in Eq. 10b. In the presence of an oxide film the corrosion process involves reactions between three phases and at two different interfaces. The metal oxidation half-reaction (8a) occurs at the m|ox interface and the aqueous reduction half-reaction (8b) occurs at the ox|sol interface and/or on a counter electrode. The rate of each redox half-reaction can still be expressed using the Butler-Volmer equation (Eq. 11). However, not all of the free energy of reaction is available due to the potential barrier of the oxide film, $\Delta V_{oxide}(t)$:

$$\eta_{rdx\#}(t) = \eta_{ox\#}(t) = -\eta_{red\#}(t) = \left(E_{elec}(t) - E_{rdx\#}^{eq} \right) - \Delta V_{oxide}(t) \qquad (12)$$

Thus, the rate of metal oxidation depends strongly on how the thermodynamic driving force is distributed between the two interfaces and across the oxide film.

For each possible metal/metal cation oxidation reaction, *rdx#*, in a specific solution environment the metal oxidation flux is formulated by a modified Butler-Volmer equation with the overpotential for the metal oxidation as defined in equation (12):

$$J_{M\#^{n+}}(t)|_{m|ox} = J_{rdx\#}^{eq} \cdot \left(exp\left(\frac{0.5 \cdot n \cdot F}{RT} \cdot \eta_{rdx\#}(t) \right) \right) \quad (13)$$

2.5 Potential Distribution

The potential energy for an interfacial charge transfer process is often described using the Fermi-levels (the total chemical potential of electrons (φ)) in the reacting phases. For a given interfacial redox reaction, the change in the chemical potential of electrons and the change in the chemical potential of the redox species must be the same. Although the electron potential energy scale uses a different reference point and is opposite in sign to that of the hydrogen reduction potential scale, the relative values are the same in both scales, $\Delta\varphi = -\Delta E$.

At phase equilibrium, the Fermi-levels of the two reacting phases at the interface must be the same. On a bare metal surface the Fermi-levels of the metal and solution phases at the m|sol interface must be the same, $\varphi_f^{eq} = \varphi_m^{eq} = \varphi_{sol}^{eq}$. Thus,

$$\eta_{ox\#}(t) = \varphi_m(t) - \varphi_m^{eq} \quad (14a)$$

$$-\eta_{red\#}(t) = \varphi_{sol}^{eq} - \varphi_{sol}(t) \quad (14b)$$

$$\varphi_m(t) - \varphi_{sol}(t) = E_{red}^{eq} - E_{ox}^{eq} = \Delta E_{rdx}^{eq} = E_{rdx}^{eq} \ (\mathrm{V_{SHE}}) \quad (14c)$$

These relationships are schematically presented in Figure 3. The driving force for corrosion on a bare metal surface is equivalent to the difference between the Fermi-levels of the metal and solution phases at time t, and this is the same as the difference in the equilibrium potentials of the two half-reactions. If there is no change in the electrochemical potential of the solution as corrosion progresses, the corrosion rate on a bare metal surface does not change.

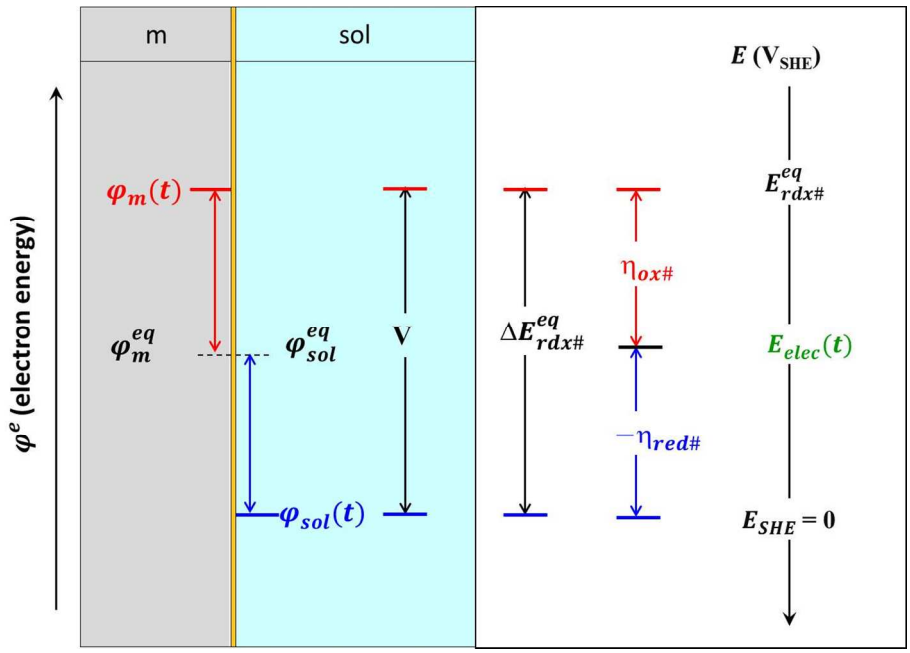

Figure 3: Relative positions of the redox reaction potentials at time t during corrosion on a bare metal surface. The potential drops across the double layer and diffusion layer are not considered for simplicity.

The Fermi level in the solution at equilibrium is the electron energy level where the density of unoccupied electron energy states ($\varphi_{E(Ox)}$) and the density of occupied electron energy states ($\varphi_{E(\mathrm{Red})}$) are the same. In the presence of an oxide, the Fermi-levels of the solution and the oxide at the ox|sol interface must be the same. The Fermi level in the metal phase at equilibrium is the electron energy level where the density of unoccupied electron energy states ($\varphi_{E(M^{n+})}$) and the density of occupied electron energy states ($\varphi_{E(M)}$) are the same. In the presence of an oxide film the Fermi-levels of the metal and the oxide at the m|ox interface must be the same. The questions are then, "What is the Fermi gap across the oxide layer?" and "Is this gap constant across the oxide layer during corrosion?"

Most of the transition metal oxides present on corroding surfaces exhibit semiconducting properties[17]. The Fermi level of a pure n-type semiconductor lies closer to the lowest energy of the conduction band, φ_{CB}, whereas the Fermi level of a pure p-type semiconductor lies closer to the highest energy of the valence band, φ_{VB}. In order for corrosion to progress at any appreciable rate, the Fermi-level of the metal at the interface must lie above the φ_{CB} of the semiconducting oxide while the Fermi-level of the solution phase must lie below the φ_{VB} of the oxide:

$$\varphi_m(t) > \varphi_{CB} \text{ and } \varphi_{sol}(t) < \varphi_{VB} \tag{15}$$

These conditions reduce the overpotential that is available for metal oxidation or solution reduction:

$$\eta_{ox}(t) = \varphi_m(t) - \varphi_m^{eq} - \Delta\varphi_{oxide}(t) \quad \text{for a p-type semiconductor} \tag{16a}$$

$$\eta_{red}(t) = \varphi_{sol}(t) - \varphi_{sol}^{eq} + \Delta\varphi_{oxide}(t) \quad \text{for an n-type semiconductor} \tag{16b}$$

The mass and charge balance conditions further dictate that the effective overpotentials for the metal oxidation and its coupled solution reduction are related as given in Eq. (13). Thus, for both n-type and p-type semiconductors,

$$\eta_{rdx}(t) = \eta_{ox}(t) + \left(-\eta_{red}(t)\right) = \varphi_m(t) - \varphi_{sol}(t) - \Delta\varphi_{oxide}(t)$$

$$= E_{rdx}^{eq} - \Delta V_{oxide}(t) \tag{17}$$

These relationships are schematically presented in Figure 4. (Here the potential drops across the space charge layers such as Mott-Schottky and double layers are not considered for simplicity. On a corroding surface these barriers should be negligible compared to the potential barrier of the oxide film.)

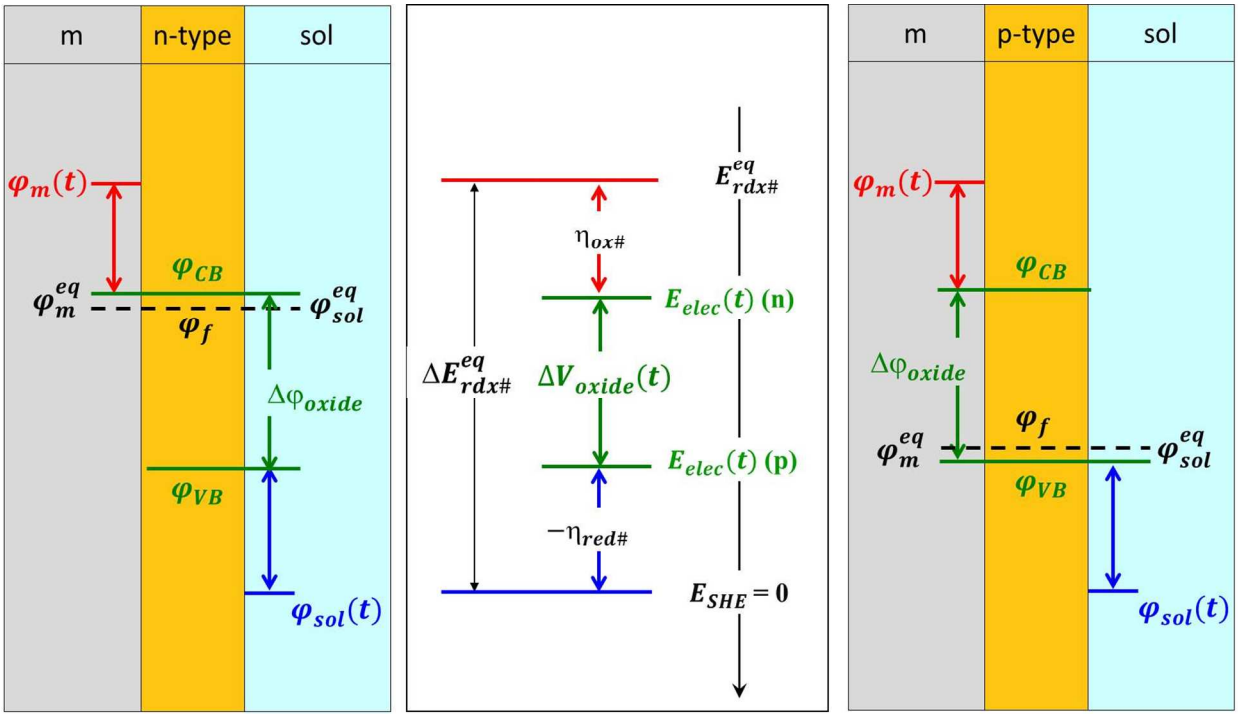

Figure 4: Relative positions of the reaction potentials at a time t during corrosion: (middle panel) on the reduction potential scale ($E(V_{SHE})$), (left panel) for an n-type film on the electron energy scale (φ^e), and (right panel) for a p-type film on the electron energy scale (φ^e).

On a pure semiconductor, the potential drop, $\Delta\varphi_{oxide}(t)$, is the band gap (V_{bg}). If the oxide film is a pure phase the band gap does not change with an increase in oxide thickness and the growth of that oxide should not affect the interfacial charge transfer rate. This can explain some of the observations where the potential drop across an oxide film is independent of oxide thickness and justifies this assumption in the Cabrera-Mott model[4]. However, typically the oxide film composition on a corroding surface will not be uniform. Instead, there will be a charge distribution within the oxide lattice; the M^{n+} concentration will be higher nearer the m|ox interface and the O^{2-} concentration will be higher nearer the ox|sol interface. Therefore, the oxide near the m|ox interface will behave more like a p-type semiconductor (due to doping of the positive charges) while near the ox|sol interface the oxide will behave more like an n-type

semiconductor (due to doping of the negative charges). The oxide film present on a corroding surface will then behave like a p-n junction in a solid-state diode device.

In the absence of any external potential the Fermi levels of two reacting phases at the reaction interface must be the same. At equilibrium (no external force) the φ_{CB} of the p-type semiconductor is higher than the φ_{CB} of the n-type semiconductor. This results in a potential barrier to the flow of electrons (the majority of charge carriers). Similarly, holes cannot flow forward (from p-type to n-type regions) unless a positive external potential (V_{ext}) is applied to overcome the potential barrier across the junction, and this potential barrier (V_j, the junction potential) is not the band gap (V_{bg}). Only when V_{ext} is larger than V_j and the Fermi-level in the n-type semiconductor region is raised above the φ_{CB} of the p-type semiconductor region can electrons flow from the n-type to p-type regions.

We can envision the potential distribution across an oxide film on a corroding surface as being similar to that in a p-n junction. In the presence of an oxide layer, the corrosion redox reaction can occur only when the potential is sufficient to overcome the oxide potential barrier, $\Delta\varphi_{oxide}$ (equivalent to V_j) so that electrons can migrate from the ox|sol interface to the m|ox interface. If the potential at the m|ox interface is the same as the aqueous redox potential, there will not be any current – i.e., no metal oxidation. The potential distribution on such a corroding system is schematically shown in Figure 5.

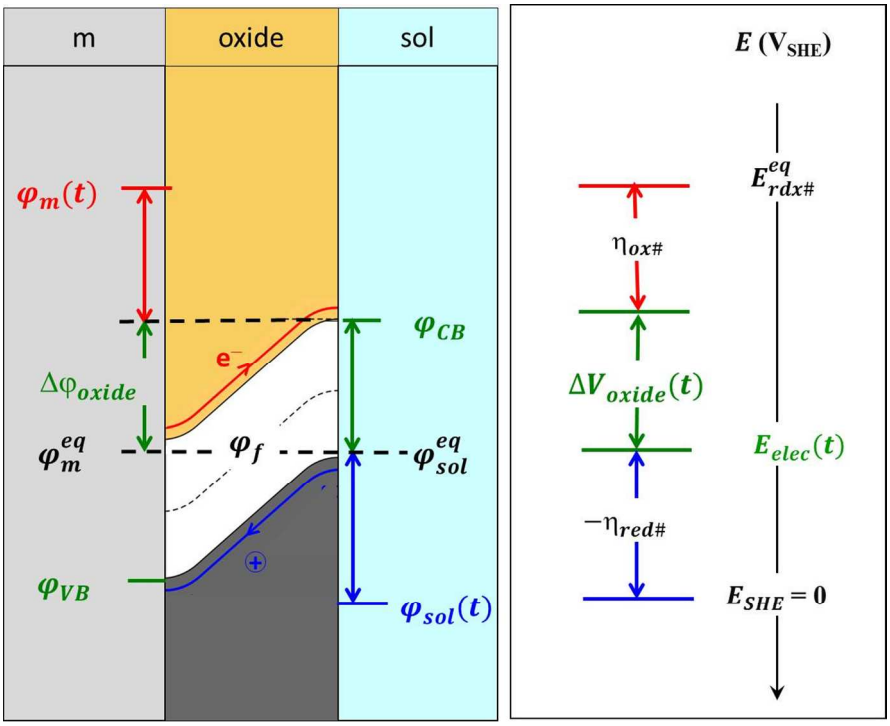

Figure 5: Relative positions of the reaction potentials at a time t during corrosion in the presence of a n-p type oxide film: (left panel) on the electron energy scale (φ^e) and (right panel) on the reduction potential scale ($E(V_{SHE})$).

Figure 5 presents the potential energy distribution on a corroding surface at a specific time under a specific solution redox condition. If the oxide grows as corrosion progresses the potential barrier across the oxide film increases. For a system where a specific metal oxidation coupled with a specific aqueous reduction reaction that leads to growth of a specific oxide film, MO#, it is reasonable to assume that $\Delta V_{oxide}(t)\left(= -\Delta\varphi_{oxide}(t)\right)$ is proportional to the changing oxide thickness:

$$\Delta V_{oxide}(t) = \Delta V_{oxide}(0) + \Delta V_{MO\#}(t) \quad (18a)$$

$$\Delta V_{MO\#}(t) = \varepsilon_{MO\#} \cdot L_{MO\#}(t) \quad (18b)$$

where $\Delta V_{oxide}(0)$ is the potential drop over, if present, the pre-existing oxide layer, $\varepsilon_{MO\#}$ is the proportionality constant or the specific potential gradient (potential drop per unit length) of oxide MO# and $L_{MO\#}(t)$ is the thickness of oxide MO# grown over time t.

Since the reaction potential energy is distributed such that it will satisfy the mass and charge balance requirements, the effective overpotential for metal oxidation will change according to Eq. (17). For a given solution redox condition where $E_{rdx\#}^{eq}$ is constant, the potential gaps at the two interfaces and across the oxide film at two different times are schematically shown in Figure 6. For simplicity $\Delta V_{oxide}(0)$ is assumed to be zero. This schematic also illustrates that even with a constant solution redox environment, as the oxide layer thickens the corrosion potential, E_{corr}, which is the Fermi-level at pseudo equilibrium (or steady state), increases. This occurs even though the effective overpotential and, hence, the rate of the metal oxidation decreases. If the electrode potential, E_{app}, instead of E_{rdx}^{eq}, is maintained constant, as is the case for potentiostatic polarization, the effective overpotential for metal oxidation decreases as the oxide grows, as schematically shown in Figure 7.

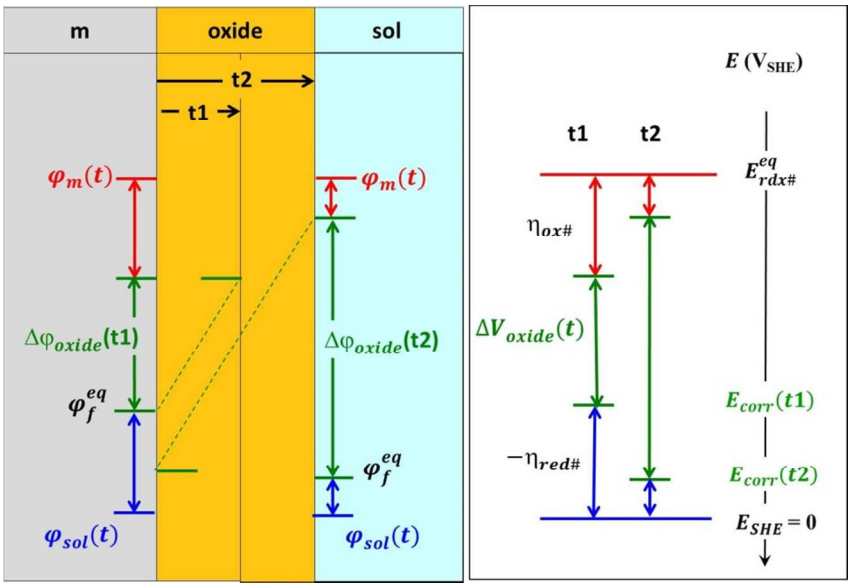

Figure 6: Effect of linear oxide growth on the potential distribution in a corroding system: (left panel) on the electron energy scale (φ^e) and (right panel) on the reduction potential scale ($E(V_{SHE})$).

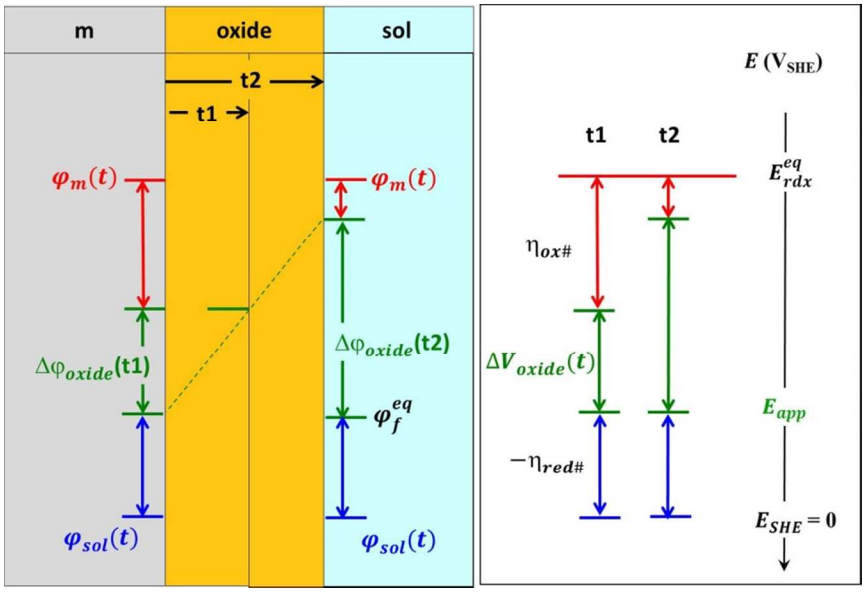

Figure 7: Effect of linear oxide growth on the potential distribution during potentiostatic polarization: (left panel) on the electron energy scale (φ^e) and (right panel) on the reduction potential scale ($E(V_{SHE})$).

The potential energy diagrams presented in Figures 5 to 7 address a system where there is only one redox reaction occurring. In a real system for an alloy with multiple elements, there may be multiple redox reactions that occur in parallel or in series. Nevertheless, the same principles apply to each individual redox reaction (rdx#) with its own electrochemical equilibrium potential, $E_{rdx\#}^{eq}$. The existence of multiple redox reactions is also the reason that E_{corr} depends on the aqueous redox environment and the type(s) of oxide that can be formed.

2.6 Formulation of the Oxide Growth and the Dissolution Fluxes

The electric potential barrier across the oxide film is an important rate controlling parameter. As discussed above, for a specific redox reaction that leads to a specific oxide film, it is reasonable to assume that $\Delta V_{MO\#}(t)$ is proportional to the oxide thickness, $L_{MO\#}(t)$ (Eq. 18). The oxide growth flux and the time dependence of $L_{MO\#}(t)$ can be established as follows. Oxide formation will compete with dissolution for the metal cations. Assuming that both processes

have a first order dependence on [M#$^{n+}$] with rate constants, $k_{MO\#}$ and $k_{diss\#}$, respectively, the mass balance requirement results in:

$$J_{MO\#}(t)|_{oxide} = f_{k-MO\#}(t) \cdot J_{M\#^{n+}}(t)|_{m|ox} \quad (20)$$

$$J_{diss\#}(t)|_{sol} = \left(1 - f_{k-MO\#}(t)\right) \cdot J_{M\#^{n+}}(t)|_{m|ox} \quad (21)$$

$$f_{k-MO\#}(t) = \left(\frac{k_{MO\#}(t)}{k_{MO\#}(t) + k_{diss\#}}\right) \quad (22)$$

The ratio of the rate constants, $f_{k-MO\#}(t)$, depends strongly on pH and temperature. An increase in temperature will increase both the oxide formation and the dissolution rates whereas a change in pH will primarily affect the dissolution rate.

Oxide formation is a chemical reaction and its rate constant can be assumed to have a normal Arrhenius dependence on the activation energy for the reaction. The electric potential energy gap across the oxide layer ($\Delta V_{MO\#}(t)$) contributes to the activation energy for the formation of an oxide (MO#) ($\Delta Ea_{MO\#}(t)$):

$$\Delta Ea_{MO\#}(t) = \Delta Ea_{MO\#}(0) + c' \cdot \Delta V_{MO\#}(t) = \Delta Ea_{MO\#}(0) + c_{MO\#} \cdot L_{MO\#}(t) \quad (23)$$

where c' is the dependency of activation energy of oxide growth of the potential drop across a layer of MO# and $c_{MO\#}$ is the specific activation energy gradient of oxide. The activation energy for the oxide formation increases as the oxide grows and the rate constant for the oxide formation decreases accordingly:

$$k_{MO\#}(t) = k_{MO\#}(0) \cdot exp\left(-\frac{c_{MO\#} \cdot L_{MO\#}(t)}{RT}\right) \quad (24a)$$

where $k_{MO\#}(0) = k_{0-MO\#} \cdot exp\left(-\frac{(\Delta Ea_{MO\#}(0))}{RT}\right)$ (24b)

(Note that the other contributors to the reaction activation energy are included in $\Delta Ea_{MO\#}(0)$ and the value of $k_{0-MO\#}$ which is the pre-exponential factor for the oxide formation, and they are assumed to be constant with time.)

The fluxes calculated in the model are related to physical parameters that can be measured. For example, the metal oxidation flux, $J_{M\#^{n+}}(t)|_{m|ox}$, can be measured as anodic current if metal oxidation current can be effectively separated from the water reduction current in an electrochemical cell:

$$i_{ox\#}(t) = n \cdot F \cdot J_{M\#^{n+}}(t)|_{m|ox} \quad (25)$$

The dissolution flux, $J_{diss\#}(t)|_{sol}$, is related to the amount of dissolved metal:

$$A_{sol} \cdot (J_{diss\#}(t)|_{sol}) \cdot dt = dm_{diss\#}(t) \quad (26)$$

where $dm_{diss\#}(t)$ represents the amount of dissolved metal over time dt (mol) and A_{sol} is the surface area exposed to solution (cm^2). The oxide growth flux, $J_{MO\#}(t)|_{oxide}$, is related to the thickness of the oxide:

$$\upsilon_{MO\#} \cdot (J_{MO\#}(t)|_{oxide}) \cdot dt = dL_{MO\#}(t) \quad (27)$$

where $\upsilon_{MO\#}$ is the molar volume of MO# ($cm^3 \cdot mol^{-1}$).

Equation (24) shows that the rate constant for oxide formation decreases exponentially with increase in oxide thickness. If the metal oxidation flux does not depend on oxide thickness, the oxide grows at a progressively slower rate (exponentially slower with time). However, since the metal oxidation flux also decreases exponentially with oxide thickness (Eqs. (11c), (13a) and (18)), the slower rate of oxide growth with time also slows down the rate of decrease in metal oxidation flux with time (Eq. (23)). As derived in more detail in the Electronic supplementary information (ESI), the net effect is that the oxide thickness can be approximated to increase logarithmically with time under a constant electrode potential ($E_{elec}(t)$) condition (i.e., constant E_{corr} or E_{app}):

$$L_{MO\#}(t) \approx \frac{1}{\lambda_{MO\#}} (ln(\lambda_{MO\#} \cdot J_{MO\#}'') + \ln t) \quad (28a)$$

$$\lambda_{MO\#} = \frac{0.5 \cdot n \cdot F}{RT} \cdot \varepsilon_{MO\#} \quad (28b)$$

$$J_{MO\#}" = \upsilon_{MO\#} \cdot f_{k-MO\#}(0) \cdot J_{rdx\#}^{eq} \cdot \left(exp\left(\frac{0.5 \cdot n \cdot F}{RT} \cdot \left(E_{elec}(t) - E_{ox\#}^{eq} - \Delta V_{oxide}(0) \right) \right) \right)$$

(28c)

$$f_{k-MO\#}(0) = \left(\frac{k_{MO\#}(0)}{k_{MO\#}(0) + k_{diss\#}} \right) \quad (28d)$$

where $\lambda_{MO\#}$ represents a constant related to the potential drop across a unit length of the layer of oxide in inverse-length equivalent units, and $J_{MO\#}"$ represents the constant component of the metal cation flux.

The approximated analytical solution of the flux equations in the MCB model (equation 28a) has the form that we recognize for logarithmic film growth as previously reported by McDonald in his PDM model[6]. They expressed the rate law for film growth (for $L_{MO\#}(t) > 5\ \dot{A}$) as

$$L_{MO}(t) \approx \frac{1}{2K}\left(ln\left(2K \cdot A \cdot (B-1) \right) + \ln t \right) \quad (29)$$

where *K, A* and *B* are constants. That their derivation for the oxide growth rate is based on very different physical and chemical descriptions, but results in the same rate expression, suggests that the simpler approach used in the MCB model is sound.

2.7. Summary of the Mathematical Formulation of Model and Model Parameters

The MCB model is summarized in Table 1. It consists of three key flux equations: metal oxidation flux, $J_{M\#^{n+}}(t)|_{m|ox}$, and metal oxide growth flux, $J_{MO\#}(t)|_{oxide}$ and metal cation dissolution flux, $J_{diss\#}(t)|_{sol}$. Due to mass and charge balance requirements the oxide growth and dissolution fluxes cannot vary independently, and their sum must be the same as the metal oxidation flux. Thus, the MCB model consists of really only two independent flux equations. These flux equations are applied to each redox pair (designated with # in the flux equation) of metal oxidation and solution reduction.

Table 1: Mathematical Formulation of the Model.

	Flux Equations used in the Model	Model Output
1	$J_{M\#^{n+}}(t)\|_{m\|ox} = J_{rdx\#}^{eq} \cdot \left(exp\left(\frac{0.5 \cdot n \cdot F}{RT} \cdot \eta_{ox\#}(t)\right)\right)$	Current (t) $i_{ox\#}(t) = n \cdot F \cdot J_{M\#^{n+}}(t)\|_{m\|ox}$
2	$J_{MO\#}(t)\|_{oxide} = \left(\frac{k_{MO\#}(t)}{k_{MO\#}(t) + k_{diss\#}}\right) \cdot J_{M\#^{n+}}(t)\|_{m\|ox}$	Oxide thickness (t) $L_{MO\#}(t) = \upsilon_{MO\#} \cdot \int_{t=0}^{t} (J_{MO\#}(t)\|_{oxide}) \cdot dt$
3	$J_{diss\#}(t)\|_{sol} = J_{M\#^{n+}}(t)\|_{m\|ox} - J_{MO\#}(t)\|_{oxide}$	Dissolved amount (t) $m_{diss\#}(t) = A_{sol} \cdot \int_{t=0}^{t} (J_{diss\#}(t)\|_{sol}) \cdot dt$
	Time Dependent Terms in the Flux Equations	Model Parameters
1	$\eta_{rdx\#}(t) = E_{red\#}^{eq} - E_{ox\#}^{eq} - \Delta V_{oxide}(t)$ $\eta_{ox\#}(t) = E_{elec}(t) - E_{ox\#}^{eq} - \Delta V_{oxide}(t)$	$J_{rdx\#}^{eq}$, $E_{red\#}^{eq}$, $E_{ox\#}^{eq}$
2	$\Delta V_{oxide}(t) = \Delta V_{oxide}(0) + \varepsilon_{MO\#} \cdot L_{MO\#}(t)$	$\Delta V_{oxide}(0)$, $\varepsilon_{MO\#}$, $\upsilon_{MO\#}$
3	$\Delta Ea_{MO\#}(t) = \Delta Ea_{MO\#}(0) + c_{MO\#} \cdot L_{MO\#}(t)$	$\Delta Ea_{MO\#}(0)$, $c_{MO\#}$
4	$k_{MO\#}(t) = k_{MO\#}(0) \cdot exp\left(-\frac{c_{MO\#} \cdot L_{MO\#}(t)}{RT}\right)$	$k_{MO\#}(0)$, $k_{diss\#}$

In the MCB model these flux equations are formulated based on well-established classical rate equations. The metal oxidation flux is formulated using a modified Butler-Volmer equation with an effective overpotential, where the effective overpotential takes into account the decrease in the driving force due to the potential drop across the oxide layer that is present or growing during corrosion. The oxide growth flux is formulated based on a first-order dependence of the

oxide formation on the metal cation flux, and on an Arrhenius dependence of the rate constant on activation energy, which increases with an increase in the potential drop across the oxide layer. The metal ion dissolution flux is simply the difference between the metal oxidation flux and the metal oxide growth flux. The ratio of the oxide growth flux to the dissolution flux is determined by their rate constants. The rate constant of the oxide growth changes with time as the oxide grows while the rate constant for dissolution from a given oxide surface is constant with time.

In the MCB model, the model parameters are: (1) the equilibrium potentials of the two coupled half-redox reactions ($E_{red\#}^{eq}$ and $E_{ox\#}^{eq}$), (2) the potential drop over the initially present oxide layer ($\Delta V_{oxide}(0)$) and the specific potential drop over the MO# oxide that is growing ($\varepsilon_{MO\#}$), and (3) the rate constant for MO# oxide formation without an oxide barrier ($k_{MO\#}(0)$). The last term can be further divided into two more fundamental parameters, a pre-exponential factor and an activation energy ($k_{0-MO\#}$ and $\Delta Ea_{MO\#}(0)$). These model parameters for a given alloy depend on the corrosion environment (which includes the type and concentration of aqueous redox species present, pH and temperature). The effects of the environmental parameters on the overall corrosion kinetics are thus modeled through their effects on the model parameters.

The flux equations can be numerically solved using any standard computer software differential equation solver. The results presented below were obtained using MATLAB.

3. EXAMPLES OF MODEL SIMULATION RESULTS

The fluxes that the MCB model calculates correspond to measurable quantities, the current, the oxide thickness and the amount of dissolved metal as a function of corrosion time. These are all independently measurable quantities and the model's capability for predicting corrosion kinetics over a wide range of environmental conditions can be verified experimentally.

We have applied the MCB model to simulate the potentiostatic polarization of a number of alloys including carbon steel, stainless steel, Co-Cr alloy Stellite 6, and Fe-Ni-Cr alloys Inconel 600 and Alloy 800. The preliminary results are very promising in all cases modelled to date and a few examples are presented here.

3.1 Oxide Thickness on Pure Iron

We have applied the MCB model to predict the thickness of iron oxide grown as a function of E_{app} and compared the results to experimental data obtained from potentiostatic polarization of pure iron in mildly basic solutions by Sato *et al.*[14]. The model simulation results and the experimental data are compared in Figure 8, showing an excellent agreement. For this simulation, following parameters were used: $i^{eq}_{Fe3O4} = 6\times10^{-6}$, $f_{k-MO\#}(0) = 0.9$, $\upsilon_{MO\#} = 30$ and $E^{eq}_{ox\#}$ was calculated based on the Eq. 5 of Sato's work[19].

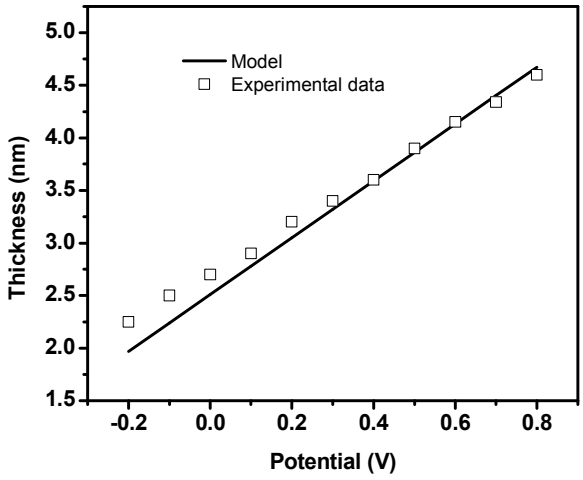

Figure 8: Measured average oxide thickness on pure iron after 1 h potentiostatic polarization at 25 °C in a range of pHs from 7.45 to 10.45 in 0.15 N boric-borate solution (symbols are data from Table 2 of Ref. [14]). The straight line is the prediction of the MCB model at pH=10.45. (Note that Sato's work showed no dependence of oxide thickness on pH over the range studied.)

3.2 Corrosion of Cr-containing Alloys

Model simulations and the results of polarization tests (at −0.6 V_{SCE}) of two alloys, Co-Cr (Stellite 6) and Fe-Ni-Cr (Alloy 800), are shown in Figure 9. The tests were performed at two different pHs, 10.6 and 8.4, in 0.01 M borate buffer solutions at 25 ^{o}C. The polarization potentials modelled are near the corrosion potentials measured on these alloys in deaerated solutions[ref]. The model predictions of the current behaviour are in very good agreement with the data.

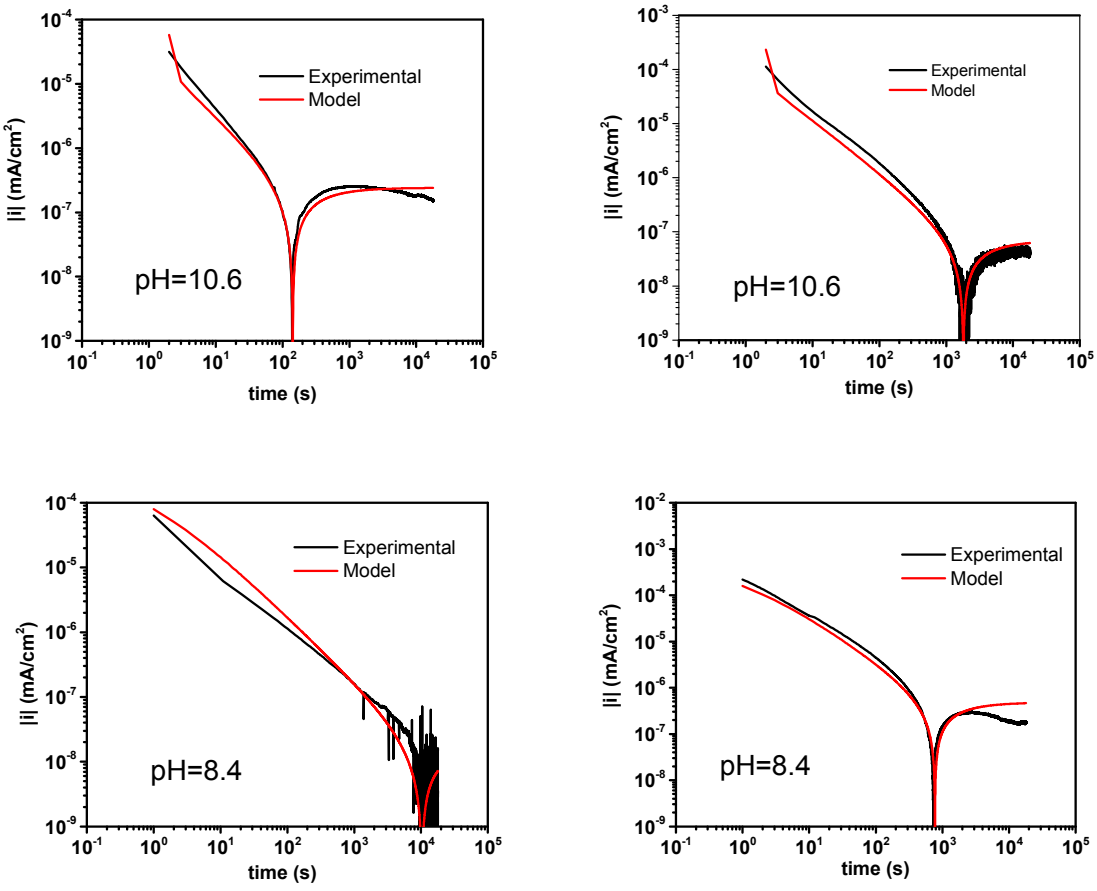

Figure 9: Current observed during polarization at −0.6 V_{SCE} of (left panel) Co-Cr alloy Stellite 6 and (right panel) Fe-Ni-Cr alloy 800 at (top row) pH 10.6 and (bottom row) pH 8.4. Experimental results are in black and modelling results are in red.

In these simulations, the surface was assumed to be initially covered with a 2-nm thick layer of chromium oxide (Cr_2O_3)[20]. With this Cr_2O_3 layer present the only oxidation pathway that is thermodynamically possible at –0.6 V_{SCE} is the conversion of the chromium oxide to chromite ($CoCr_2O_4$ or $FeCr_2O_4$)[15]. (When this conversion is complete Fe_3O_4 may grow over the chromite layer for the Fe-Ni-Cr alloy. For simplicity this process is not considered in the following discussion as it did not occur under the test conditions.) Since the solubility of chromium is much lower than that of cobalt (for the Co-Cr alloy) and iron and nickel (for the Fe-Ni-Cr alloy) under the test conditions[21], we assumed that only cobalt dissolution occurred (from the Co-Cr alloy), or that only iron dissolution occurred (from the Fe-Ni-Cr alloy). The solubility of nickel is also lower than that of iron and hence nickel dissolution from the Fe-Ni-Cr alloy at this low potential was not modeled. Nevertheless, the oxidative conversion of Cr_2O_3 to chromite requires additional modeling considerations.

Alloys which contain more that about 10% Cr typically display corrosion resistance because of the presence of a thin protective layer of air-formed Cr_2O_3 on the surface. This is the case for the Fe-Cr-Ni and Co-Cr alloys that we have studied. Mott[3] has shown that there can be a 5-nm maximum thickness of chromium oxide formed after long time of exposure to room temperature air. Even in deaerated solutions ($E_{corr} \approx$ –0.48 V_{SCE} and –0.59 V_{SCE} on Stellite 6 in deaerated solutions at pH 10.6 and 8.4, respectively[21]), this chromium oxide is converted to a mixed element chromate layer ($CoCr_2O_4$ for cobalt alloys and $FeCr_2O_4$ for Fe-Cr-Ni alloys):

$$M + Cr_2O_3 + 2\ OH^- \rightarrow MCr_2O_4 + H_2O + 2\ e^- \qquad \text{on WE} \qquad (30a)$$

$$Ox + n\ e^- \rightarrow Red \qquad \text{on CE} \qquad (30b)$$

While this occurs there are two types of oxide in the oxide film: a more chromite-like layer and a more chromium oxide-like layer.

During conversion of chromium oxide to chromite, the thickness of the chromium oxide layer decreases while that of the chromite layer increases correspondingly[20]:

$$L_{Cr2O3}(t) = L_0 - f_l \cdot L_{MCr2O4}(t) \quad (31)$$

where $L_{Cr2O3}(t)$ and $L_{MCr2O4}(t)$ are the thicknesses of the chromium oxide and chromite layers, L_0 is the initial air-formed chromium oxide thickness. The factor f_l is used to adjust for differences in the unit cell lengths of Cr_2O_3 and chromite oxide. In actuality there may not be a sharp division of the oxide into two distinct layers but a gradation between the two oxide types. In the model the oxide thicknesses in equation (32) are for pure-oxide-phase equivalent thicknesses. The potential drop across the film can then be expressed as:

$$\Delta V_{oxide}(t) = \varepsilon_{Cr2O3} \cdot L_{Cr2O3}(t) + \varepsilon_{MCr2O4} \cdot L_{MCr2O4}(t) \quad (32)$$

$$\Delta V_{oxide}(t) = \varepsilon_{Cr2O3} \cdot L_0 + (\varepsilon_{MCr2O4} - f_l \cdot \varepsilon_{Cr2O3}) \cdot L_{MCr2O4}(t) \quad (33)$$

where and ε_{Cr2O3} and ε_{MCr2O4} are the specific potential drops across the different oxide layers, respectively. The specific potential drop, $\varepsilon_{MO\#}$, is characteristic of the oxide[9] (with a value in the range of 10^5 to 10^7 V·cm^{-1}). The values for ε_{Cr2O3} and ε_{MCr2O4} are not known and the values used in the simulations were those that yielded best fits of data on a given alloy. The values used in the simulations shown in Figure 8 are listed in Table 2. Ideally, at a given temperature these values are fixed, independent of pH and E_{app}. The best-fit values of these parameters in the MCB model are indeed nearly the same at two different pHs. The values of the other model parameters are also listed in Table 2 and discussed below.

Under potentiostatic polarization, the aqueous reduction reaction that is not coupled with metal oxidation, but coupled with aqueous oxidation on the counter electrode, can also occur on the working electrode. This aqueous reduction reaction on the working electrode is treated as a separate independent redox reaction with its own equilibrium potential (or the difference of the

equilibrium potentials of the two half-reactions of aqueous reduction and aqueous oxidation). For example, reduction of H_2O or dissolved O_2 (at an impurity level) can occur on the working electrode coupled with oxidation of H_2 or H_2O on the counter electrode:

$$2\ H_2O + 2\ e^- \rightarrow H_2 + 2\ OH^- \quad \text{on WE} \quad (31a)$$

$$H_2 + 2\ OH^- \rightarrow 2\ H_2O + 2\ e^- \quad \text{on CE} \quad (31b)$$

and/or $$O_2 + 4\ H^+ + 4\ e^- \rightarrow 2\ H_2O + 2\ e^- \quad \text{on WE} \quad (32a)$$

$$2\ H_2O \rightarrow O_2 + 4\ H^+ + 4\ e^- \quad \text{on CE} \quad (32b)$$

The aqueous redox reactions do not contribute to the metal oxidation flux or oxide growth flux, but only to the net current. Nevertheless, the aqueous reduction flux on the working electrode is expressed in a manner similar to that used for the metal oxidation flux, using an effective cathodic overpotential as a function of potential drop across the oxide layer.

Table 2: Fitting parameters for Cr-alloy potentiostatic simulations.

Alloy system	pH	i^{eq}_{MCr2O4} (mA·cm^{-2})	i^{eq}_{aq-rdx} (mA·cm^{-2})	ε_{Cr2O3} (V·cm^{-1})	ε_{MCr2O4} (V·cm^{-1})	c_{MCr2O4}	$f_{k-MCr2O4}(0)$
Co-Cr	10.6	1.0×10^{-7}	-3.5×10^{-19}	1.7×10^{6}	5.5×10^{6}	1×10^{7}	0.91
	8.4	5.0×10^{-7}	-3.0×10^{-20}	1.2×10^{6}	5.5×10^{6}	1×10^{7}	0.15
Fe-Ni-Cr	10.6	1.0×10^{-6}	-1.0×10^{-19}	1.9×10^{6}	3.2×10^{6}	1×10^{7}	0.88
	8.4	1.0×10^{-6}	-1.0×10^{-19}	1.2×10^{6}	3.2×10^{6}	1×10^{7}	0.26

The values of the model parameters, the exchange current density (i^{eq}_{MCr2O4}) for the metal oxidation (30) and the exchange current ($i^{eq}_{aq-rdx\#}$) for the solution redox reaction (31, 32) and the initial rate constants ratio $f_{k-MO\#}(0)$ are also listed in Table 2. Although these values were obtained from best fits to the data, these values are nearly the same for a given alloy and all within acceptable ranges. The exchange current densities depend on the solution conditions and factors related to the surface characteristics. The larger variation in the exchange currents on

Stellite 6 due to pH change can be attributed to the presence of two alloy phases, Cr-rich and Co-rich phases, on Stellite 6.

The ratio $f_{k-MO\#}(0)$ depends on the solution environment, the type of growing oxide, and other factors, but this ratio is always less than one, and the ratio should be higher at a pH where the oxide solubility is lower. The solubilities of Fe^{2+} and Co^{2+}species are lower at pH 10.6 than at pH 8.4, and the best-fit values for the ratio $f_{k-MO\#}(0)$ do indeed reflect this pH dependence.

At a higher potential, more oxidation pathways are available. In the MCB model the individual oxidation reactions are modelled separately and their contributions are added to obtain the overall corrosion kinetics.

4. SUMMARY

In this study, a new classical model for oxide growth and metal dissolution is presented. This Mass Charge Balance (MCB) model is based on mass and charge balance and consists of three key flux equations: metal oxidation, oxide growth, and dissolution flux. The mass and charge balance requirements dictate that the oxide growth and dissolution fluxes cannot vary independently, but their sum must be the same as the metal oxidation flux. The metal oxidation flux is formulated using a modified Butler-Volmer equation with an oxide-thickness-dependent effective overpotential. The oxide growth and dissolution fluxes have a first-order dependence on the metal oxidation flux. Mass balance dictates that the ratio of the oxide growth and the dissolution fluxes is determined by their respective first-order rate constants. The rate constant for oxide growth is assumed to have a normal Arrhenius dependence on the activation energy for the reaction where the potential drop across the growing oxide layer contributes to the activation energy. Thus, the rate constant for oxide growth decreases exponentially with oxide thickness

while the rate constant for dissolution remains constant. The analytical solution of this model results in a logarithmic dependence of the thickness of oxide on time.

The MCB model is able to predict the time dependent potentiostatic corrosion behaviour of both pure iron, and Co-Cr and Fe-Ni-Cr alloys.

Acknowledgments:

This research was funded under the Natural Science and Engineering Council of Canada (NSERC) and Atomic Energy of Canada Limited (AECL) Industrial Research Chair Agreement. The electrochemical analysis equipment was purchased using a grant from the Canada Foundation for Innovation.

References:

1. N. F. Mott, *Transactions of the Faraday Society*, 1939, **35**, 1175-1177.
2. N. F. Mott, *Transactions of the Faraday Society*, 1940, **35**, 472-483.
3. N. F. Mott, *Transactions of the Faraday Society*, 1947, **43**, 429-434.
4. N. Cabrera and N. F. Mott, *Reports on Progress in Physics*, 1949, **12**, 163.
5. F. P. Fehlner and N. F. Mott, *Oxid Met*, 1970, **2**, 59-99.
6. C. Y. Chao, L. F. Lin and D. D. Macdonald, *Journal of The Electrochemical Society*, 1981, **128**, 1187-1194.
7. L. F. Lin, C. Y. Chao and D. D. Macdonald, *Journal of The Electrochemical Society*, 1981, **128**, 1194-1198.
8. G. T. Burstein and A. J. Davenport, *Journal of The Electrochemical Society*, 1989, **136**, 936-941.
9. D. D. Macdonald, *Journal of The Electrochemical Society*, 1992, **139**, 3434-3449.
10. V. Battaglia and J. Newman, *Journal of The Electrochemical Society*, 1995, **142**, 1423-1430.
11. M. Bojinov, G. Fabricius, T. Laitinen, K. Mäkelä, T. Saario and G. Sundholm, *Electrochimica Acta*, 2000, **45**, 2029-2048.
12. K. Leistner, C. Toulemonde, B. Diawara, A. Seyeux and P. Marcus, *Journal of The Electrochemical Society*, 2013, **160**, C197-C205.
13. A. Seyeux, V. Maurice and P. Marcus, *Journal of The Electrochemical Society*, 2013, **160**, C189-C196.
14. N. Sato, K. Kudo and T. Noda, *Electrochimica Acta*, 1971, **16**, 1909-1921.
15. M. Behazin, J. J. Noël and J. C. Wren, *Electrochimica Acta*, 2014, **134**, 399-410.
16. Q. W. Knapp and J. C. Wren, *Electrochimica Acta*, 2012, **80**, 90-99.
17. S. Fujimoto, in *Passivation of Metals and Semiconductors, and Properties of Thin Oxide Layers*, eds. P. Marcus and V. Maurice, Elsevier Science, Amsterdam, 2006, pp. 285-290.
18. W. A. Mueller, *Canadian Journal of Chemistry*, 1960, **38**, 576-587.
19. N. Sato, T. Noda and K. Kudo, *Electrochimica Acta*, 1974, **19**, 471-475.

20. K. J. Vetter, *Electrochimica Acta*, 1971, **16**, 1923-1937.
21. A. Y. Musa, M. Behazin and J. C. Wren, *Electrochimica Acta*, 2014, **Submitted**.